Electronic Supplementary Material (ESI) for Physical Chemistry Chemical Physics.

Supplementary Information

Unraveling the initial steps of the ignition chemistry of the hypergolic ionic liquid 1-ethyl-3-methylimidazolium cyanoborohydride ([EMIM][CBH]) with nitric acid (HNO_3) exploiting chirped pulse triggered droplet merging

Souvick Biswas[a], Ivan Antonov[a], Kazuumi Fujioka[a], Grace L. Rizzo[a], Steven D. Chambreau[b], Stefan Schneider[c], Rui Sun[a*], Ralf I. Kaiser[a*]

[a] Department of Chemistry, University of Hawai'i at Manoa, Honolulu, Hawaii 96822, United States

[b] Jacobs Technology, Inc., Edwards Air Force Base, California 93524, United States

[c] Air Force Research Laboratory, Edwards Air Force Base, California 93524, United States

* Corresponding author. E-mail: ruisun@hawaii.edu; ralfk@hawaii.edu

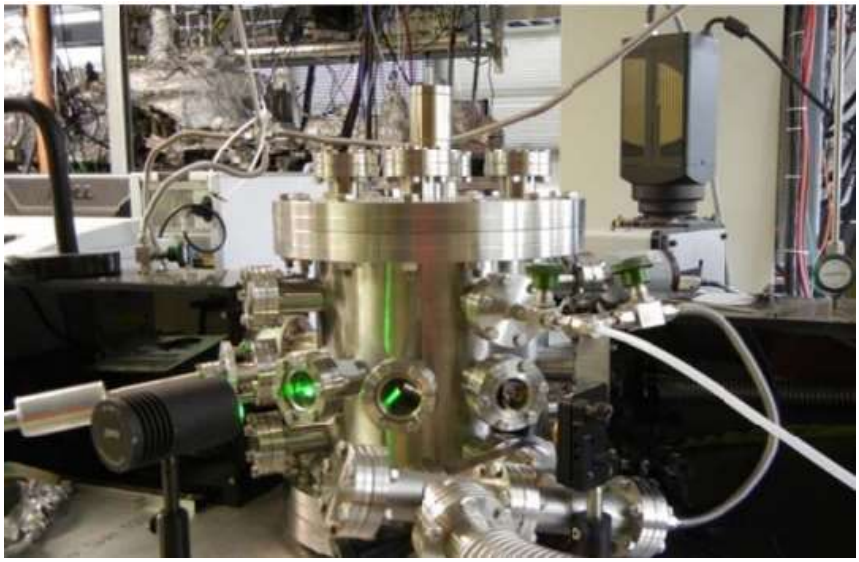

Figure S1. Side view of the levitator experimental setup exploiting the levitation device.

Table S1. Droplet sizes for the ionic liquid ([EMIM][CBH]) and HNO_3.

Droplet index	[EMIM][CBH] (μL)	HNO_3 (μL)	HNO_3 concentration used
1	16.5 ± 8.0	12.6 ± 6.0	10%
2	3.6 ± 2.0	6.6 ± 3.0	10%
3	3.8 ± 2.0	3.2 ± 2.0	10%
4	6.0 ± 3.0	9.1 ± 5.0	10%
5	13.9 ± 7.0	25.1 ± 1.3	10%
6	12.7 ± 6.0	13.0 ± 7.0	10%
1	6.6 ± 3.0	7.1 ± 4.0	20%
2	4.1 ± 2.0	7.6 ± 4.0	20%
1	22.6 ± 1.1	7.6 ± 4.0	30%
2	15.8 ± 8.0	13.4 ± 7.0	30%
3	42.2 ± 2.1	23.2 ± 1.2	30%
4	12.6 ± 6.0	19.2 ± 1.0	30%
5	28.2 ± 1.4	15.1 ± 8.0	30%
1	7.8 ± 4.0	12.8 ± 6.0	70%
2	7.6 ± 4.0	5.0 ± 2.0	70%
3	34.3 ± 1.7	9.1 ± 5.0	70%
4	23.4 ± 1.2	8.2 ± 4.0	70%
5	38.5 ± 1.9	4.4 ± 2.0	70%
6	40.5 ± 2.0	5.2 ± 3.0	70%
7	15.3 ± 8.0	11.4 ± 6.0	70%
8	10.9 ± 5.0	11.4 ± 6.0	70%

S1. Generation of merging motion due to amplitude modulation:

Let us consider a small droplet levitated slightly below a pressure node. It penetrates into a high pressure region (antinode) of the vertical standing wave until the acoustic pressure cancels the gravitational pull. Assuming that the depth of penetration is small compared to the distance between the pressure nodes, the action of the acoustic pressure can be described with the harmonic potential of the form $kz^2/2 = \omega^2 mz^2/2$, where m is the droplet mass, z is the vertical position of the droplet relative to the pressure node, $k = \omega^2 m$ is the harmonic force constant of the acoustic potential at the node, and ω is the eigenfrequency of the droplet vertical oscillations. Thus, when the droplet levitates, one can write down the following equation from the force balance: $\omega^2 mz = mg$, where $g = 9.81$ m/s^2 is the gravitational potential. From there, one can obtain expression for the vertical displacement of the droplet from the node: $z = g/\omega^2$. For the eigenfrequencies in the range of $\omega/2\pi = 20 – 40$ Hz observed in this work, $z = 0.6 – 0.15$ mm is obtained which is in a good agreement with the requirement that the depth of penetration into the antinode is small compared to the distance between the pressure nodes, i.e., $z = 0.6\text{-}0.15 \text{ mm} << \lambda/2 \approx 330/(2\times5.8\times104) = 2.8$ mm.

S2. Details of droplet merging steps:

First, one droplet of the ionic liquid ([EMIM][CBH]) was loaded in the second pressure minimum above the ultrasonic transducer; hereafter the droplet of the oxidizer HNO_3 was dispensed with a similar or slightly smaller diameter into the pressure minimum above. Second, the chirped pulse of 1 s duration with the modulation voltage of typically 600 mV was applied to tune in for the resonant frequency of the upper droplet. Initially the droplet undergoes only non-axisymmetric oscillations, which were not sufficient to de-trap or dislocate the droplet out of the acoustic potential well. Third, as soon as the resonant frequency for the axial oscillations was attained in the chirp, there occurs a deformation of the droplet, making it a prolate spheroid from an oblate one along the vertical axis. The oscillation was further amplified due to the significantly high value of modulation voltage applied. Since the resonant frequency depends on the droplet radius, the oscillations induced are found to be smaller in the lower droplet, if it is larger than the other droplet positioned above. Due to this excitation to the resonant normal mode of the droplet, it initiated a

vertical oscillation and fell under gravity into the pressure node below, where it merged with the lower droplet driven by the surface tension. The amplitude for the chirped pulse was optimized prior to actual experimental run and it was kept at a fixed value while applying the pulse. If the two droplets possess similar radii, then both can be induced into oscillation by the modulated ultrasonic wave, as a result, either the droplet in the bottom node can go up to the third node or the droplet in the third node can fall downwards to the second node, leading to formation of a merged droplet. We have observed merging events via both kinds of motion of the two droplets. When a larger droplet was loaded on the top pressure node than the bottom one, the merging was predominantly directed by the upward motion of the of the droplet from the lower node. This merging approach was suitably applied in our experiments irrespective of the relative sizes of the droplets.

S3. Pulse sequence:

The droplet merging and the subsequent physical and chemical changes occur at a very fast time scale (in milliseconds regime); therefore, each spectroscopic and visual detection methods needed to be synchronized. Hence, the data collection tools except the FTIR spectrometer were synchronized and externally triggered by a pulse generator, (Quantum Composer Plus, model-9518) operating at 1 kHz repetition rate. The merging-up chirp, which was generated by the waveform/function generator was triggered in a single-shot mode, spanning 1 s, with a typical temporal delay of 100 ms from the trigger pulse (T_0). The delay was introduced to capture the initial unperturbed droplets in the videos. The Raman excitation laser and ICCD detector were triggered in normal mode, that is, both ran continuously at 1 kHz repetition rate without any delay from the trigger shot. On the other hand, the optical and infrared camera were operated in burst mode which implies the number of pulses were limited to a certain value. As the infrared camera was only capable of operating up to one-fourth of the trigger repetition rate, it was synchronized by providing 3 milliseconds wait time with respect to the trigger (T_0), enabling to capture thermal images every fourth pulses from T_0, thus, it was synchronized with the optical video frames. Note that at these diluted concentrations of HNO_3 from 10 to 70 % no ignition took place; therefore, no UV-Vis emission spectra could be recorded.

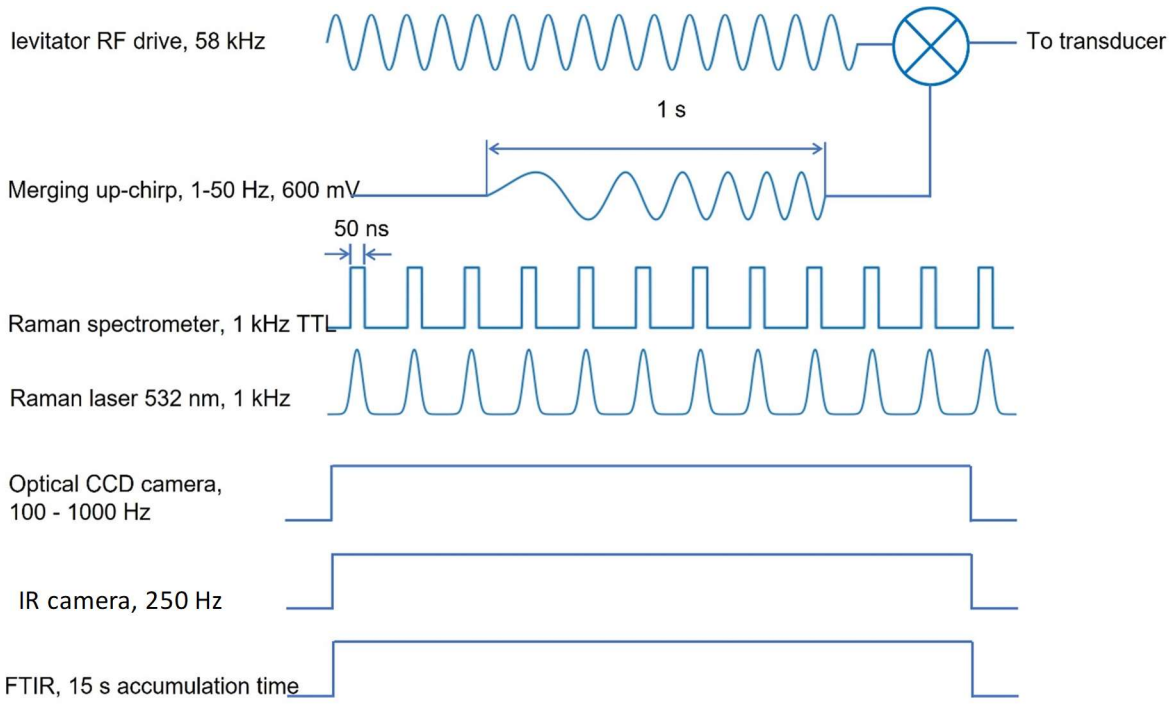

Figure S2. Typical pulse sequence used for operation of the ultrasonic levitator, droplet merging and data recording.

S4. Quantification of gas-phase products by FTIR spectroscopy:

The number densities or number of moles of the generated gases, such as hydrogen cyanide (HCN), nitrous oxide (N_2O), nitrogen dioxide (NO_2), and nitric oxide (NO) during merging events were quantified directly from the calibration curves (Figures S3-S6) obtained by taking different pressures of the respective gases individually in the process chamber maintaining the identical experimental conditions. The number densities (cm^{-3}) were calculated using the following expression:

$$\text{Number density (in cm}^{-3}) = \frac{(P\ Torr) \times 6.023 \times 10^{23} \times (f)}{62363\ cm^3 Torr\ K^{-1}\ mol^{-1} \times 298\ K}$$

Where, *P* is the pressure of the gas taken in Torr and *f* is the dilution factor of the gas used, if there is any.

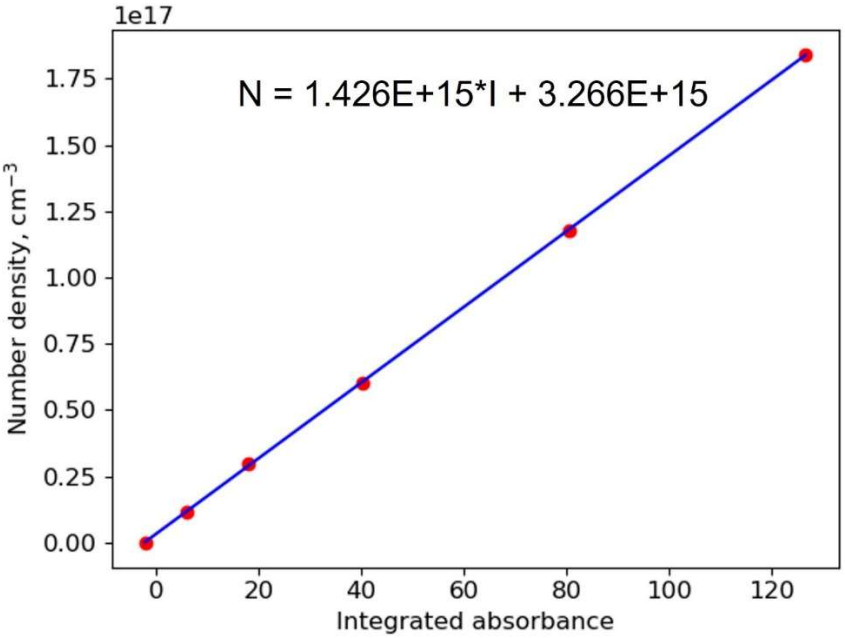

Figure S3. Calibration of FTIR signal for hydrogen cyanide (HCN). Integrated area for the CH stretch band in the 3280-3430 cm^{-1} range was used.

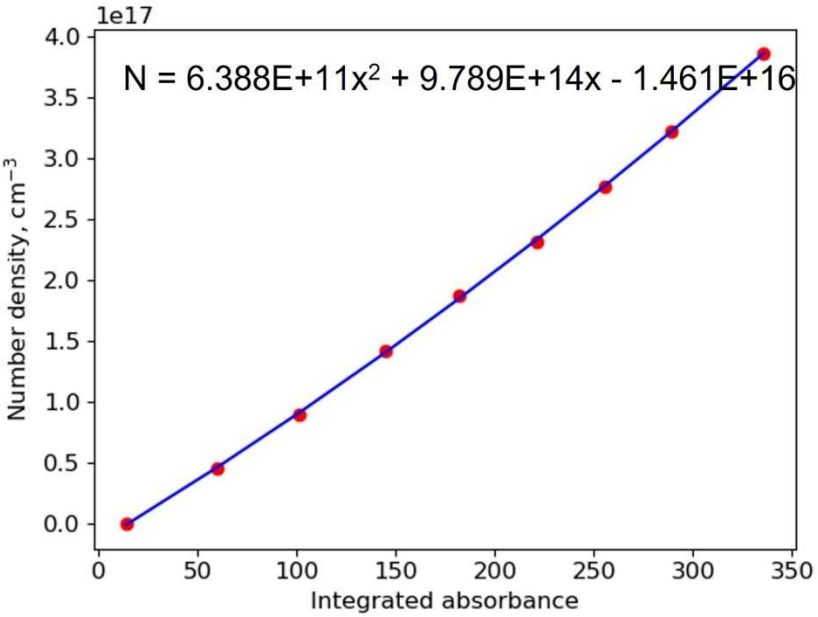

Figure S4. Calibration of FTIR signal for nitrous oxide (N_2O). Integrated area for the N=N stretch band in the 2100-2270 cm^{-1} range was used.

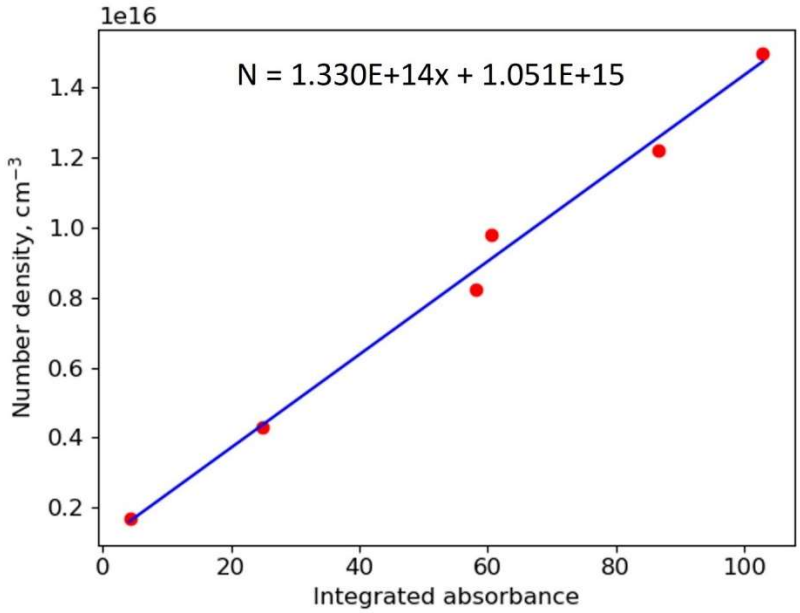

Figure S5. Calibration of FTIR signal for nitrogen dioxide (NO_2). Integrated area for the NO_2 asymmetric stretch band in the 1520-1670 cm^{-1} range was used.

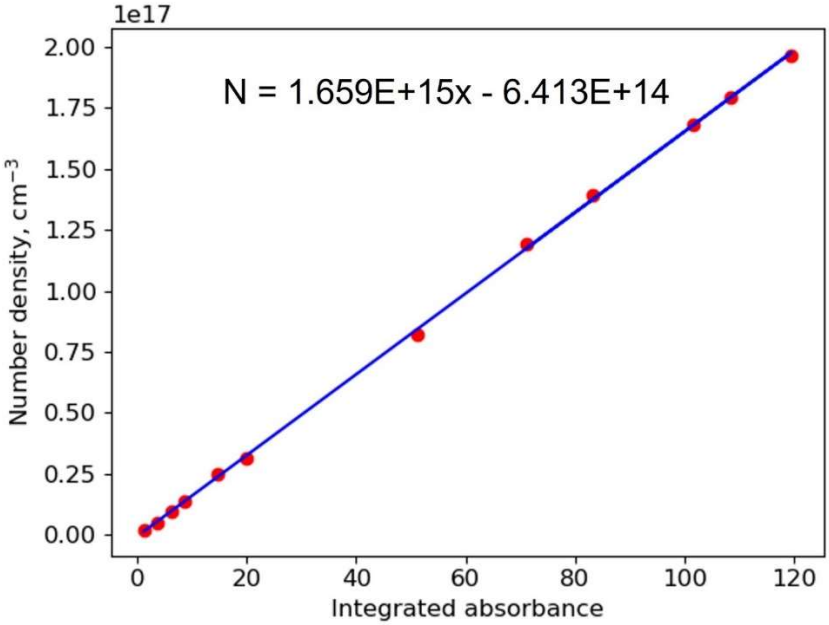

Figure S6. Calibration of FTIR signal for nitric oxide (NO). Integrated area for the NO stretch band in the 1690-1980 cm^{-1} range was used.

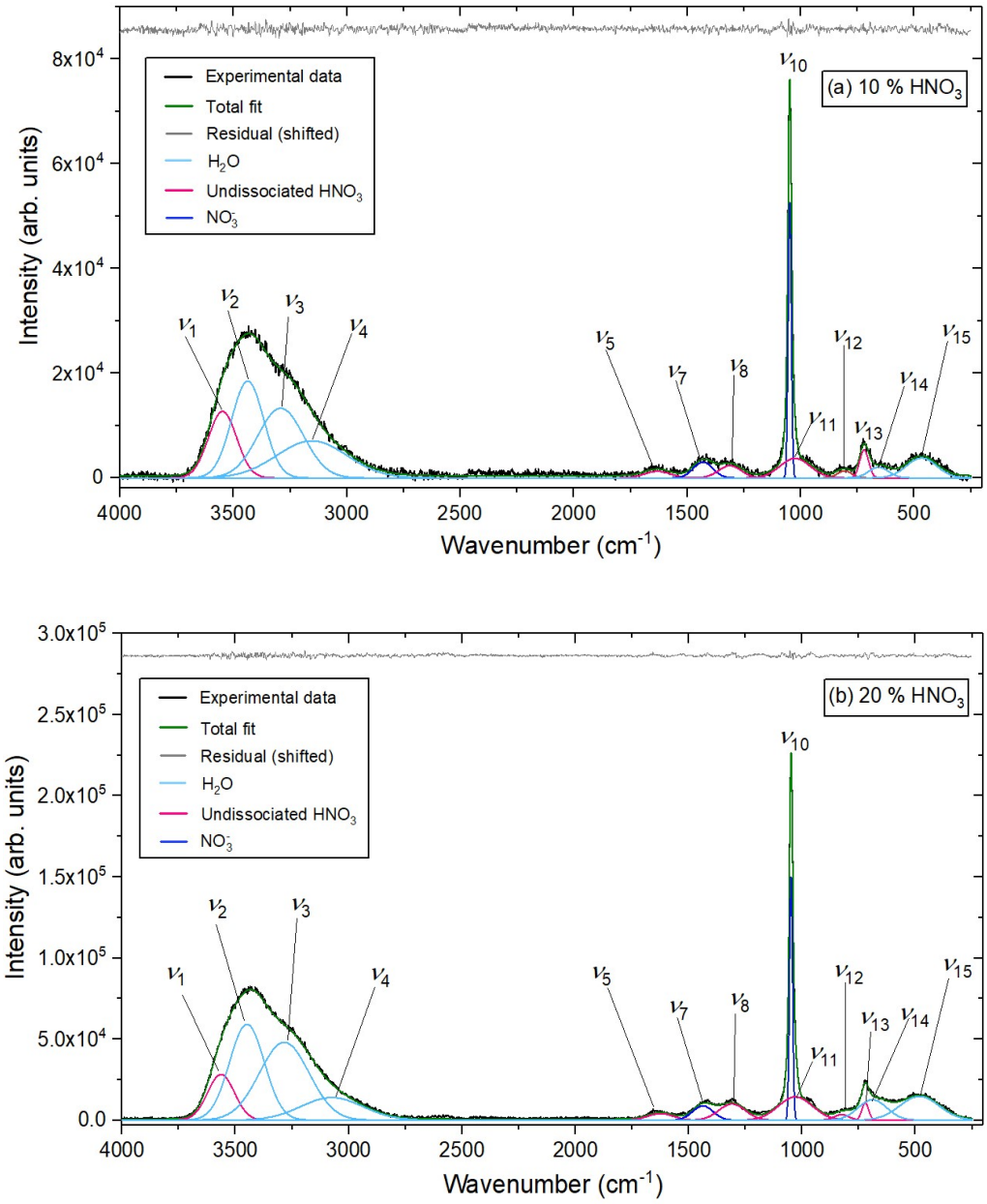

Figure S7. Raman spectra with deconvolution for the aqueous solutions of nitric acid (HNO_3) in the range 4000-200 cm^{-1} for concentrations- (a) 10 % and (b) 20 %.

Table S2: Collision energies of the reactant droplets- ionic liquid ([EMIM][CBH]) and oxidizer (HNO_3) during merging.

Strength of HNO_3 (w/w)	Volume of [EMIM][CBH] droplet (μL)	Mass of [EMIM][CBH] droplet (kg) ($\times 10^{-6}$)	Speed of approach (ms^{-1})	Total collision energy (J) ($\times 10^{-4}$)	Collision energy per mole ($J\ mol^{-1}$)
10%	12.7 ± 6.0	12.1 ± 5.7	5.2 ± 0.8	1.6 ± 0.1	2.0 ± 0.2
20%	6.6 ± 3.0	6.3 ± 2.9	5.6 ± 0.9	1.0 ± 0.1	2.3 ± 0.2
30%	28.2 ± 1.4	26.9 ± 1.3	5.0 ± 0.7	3.4 ± 0.1	1.8 ± 0.1
70%	7.8 ± 4.0	7.4 ± 3.8	5.4 ± 0.8	1.1 ± 0.1	2.1 ± 0.1

Table S3: Enthalpy changes of the reactant droplets- ionic liquid ([EMIM][CBH]) and oxidizer (HNO_3) during merging, considering the overall specific heat capacity to be 3.0 ± 0.9 $Jg^{-1}K^{-1}$. The resultant specific heat capacity of the liquid mixture was evaluated using the specific heat capacity values for similar type of ionic liquids containing $[EMIM]^+$ (2.0 $Jg^{-1}K^{-1}$) and calculated for aqueous nitric acid solutions in the range 3.6-4.1 $Jg^{-1}K^{-1}$.[1]

Strength of HNO_3 (w/w)	Mass of HNO_3 droplet (kg) ($\times 10^{-6}$)	Mass of [EMIM][CBH] droplet (kg) ($\times 10^{-6}$)	HNO_3 (mol) ($\times 10^{-5}$)	[EMIM][CBH] (mol) ($\times 10^{-5}$)	Temperature increase (K)	ΔH_{total} (kJ) ($\times 10^{-4}$)	ΔH_{mol} ($kJ\ mol^{-1}$)
10%	13.5 ± 7.3	12.1 ± 5.7	2.1 ± 1.1	8.2 ± 3.9	13.0 ± 6.3	10.0 ± 5.6	9.7 ± 7.9
20%	7.6 ± 4.3	6.3 ± 2.9	2.4 ± 1.4	4.3 ± 1.9	5.2 ± 1.4	2.1 ± 1.3	3.1 ± 1.7
30%	16.6 ± 8.8	26.9 ± 1.3	7.9 ± 4.2	18.3 ± 0.9	7.7 ± 1.8	10.4 ± 2.7	4.0 ± 0.9
70%	18.1 ± 8.5	7.4 ± 3.8	19.8 ± 9.3	5.1 ± 2.6	12.0 ± 2.1	9.7 ± 4.6	3.7 ± 1.8

Table S4: Percentage yields of the gaseous products from the corresponding reactants; [EMIM][CBH] hypergolic ionic liquid (HIL) and the acids (HNO_3 or HCl) during merging. The percentage yields in the HIL column are evaluated by (number of moles of respective gas) / (number of moles of HIL) ratios and the same for the acid column (HNO_3 or HCl) are calculated as (number of moles of respective gas) / (number of moles of HNO_3 or HCl).

Gaseous products	% yield from									
	10 % HNO_3		20 % HNO_3		30 % HNO_3		70 % HNO_3		12 % HCl	
	HIL	HNO_3	HIL	HNO_3	HIL	HNO_3	HIL	HNO_3	HIL	HCl
HCN	2.3 ± 1.2	9.0 ± 5.2	1.0 ± 0.4	1.2 ± 0.7	0.2 ± 0.1	0.5 ± 0.3	2.4 ± 1.1	0.6 ± 0.3	7.1 ± 3.1	4.3 ± 2.4
N_2O	1.5 ± 0.4	5.7 ± 2.7	1.0 ± 0.5	1.7 ± 0.9	0.2 ± 0.1	0.3 ± 0.2	2.9 ± 1.3	0.7 ± 0.4	< 0.1	< 0.1
NO_2	0.2 ± 0.1	1.0 ± 0.6	< 0.1	0.1 ± 0.1	< 0.1	< 0.1	1.9 ± 0.8	0.5 ± 0.3	-	-

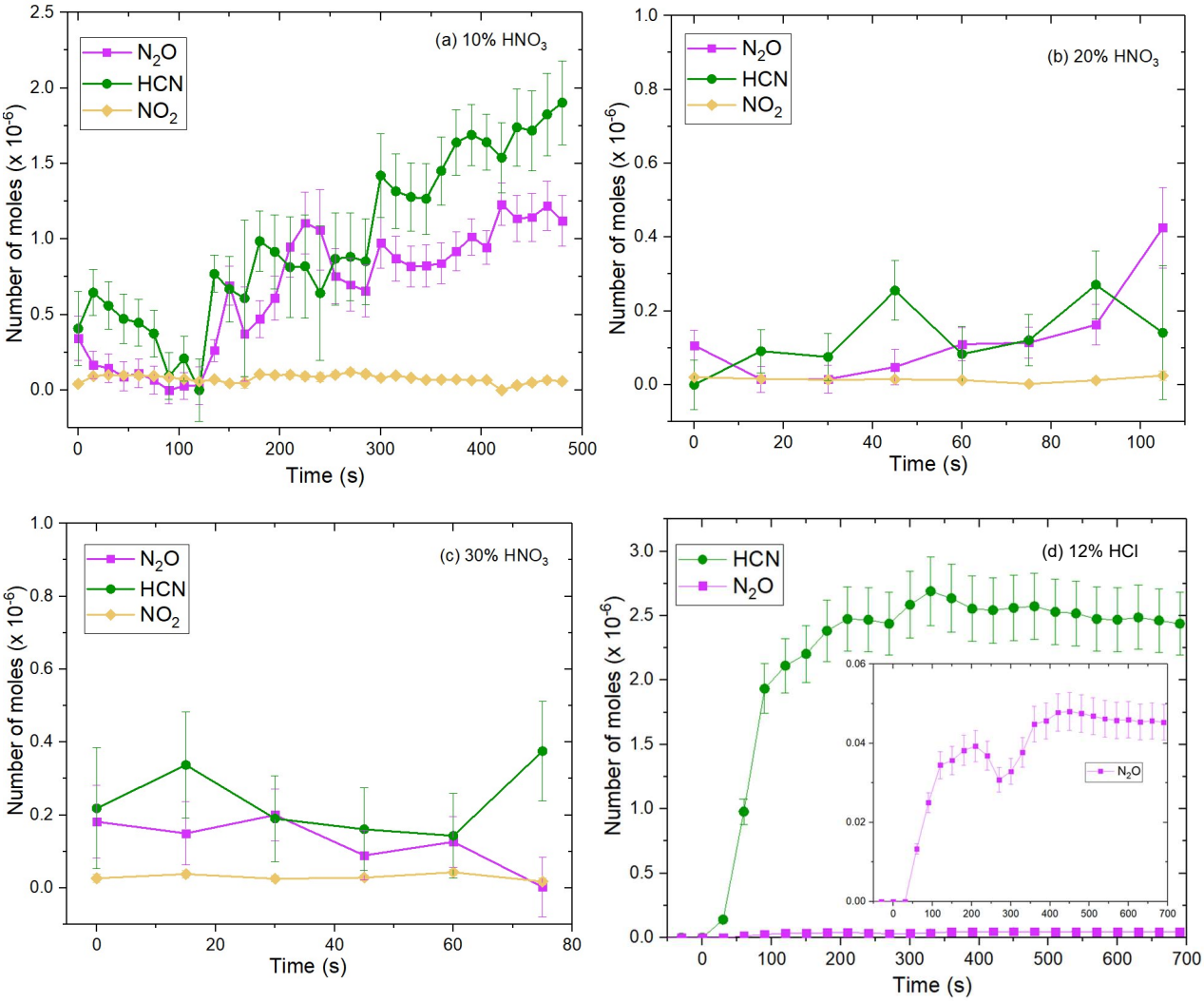

Figure S8. Temporal profiles of the gases produced after merging between the ionic liquid [EMIM][CBH] and the aqueous solution of (a-c) HNO_3 ((a) 10%, (b) 20% and (c) 30%) and (d) 12% HCl. The number of moles of the respective gases were calculated from the calibration curve considering the integrated peak area of certain characteristic bands in the FTIR spectrum of each gaseous species. After each merger, the process chamber was cleaned, evacuated, and refilled with argon inert gas.

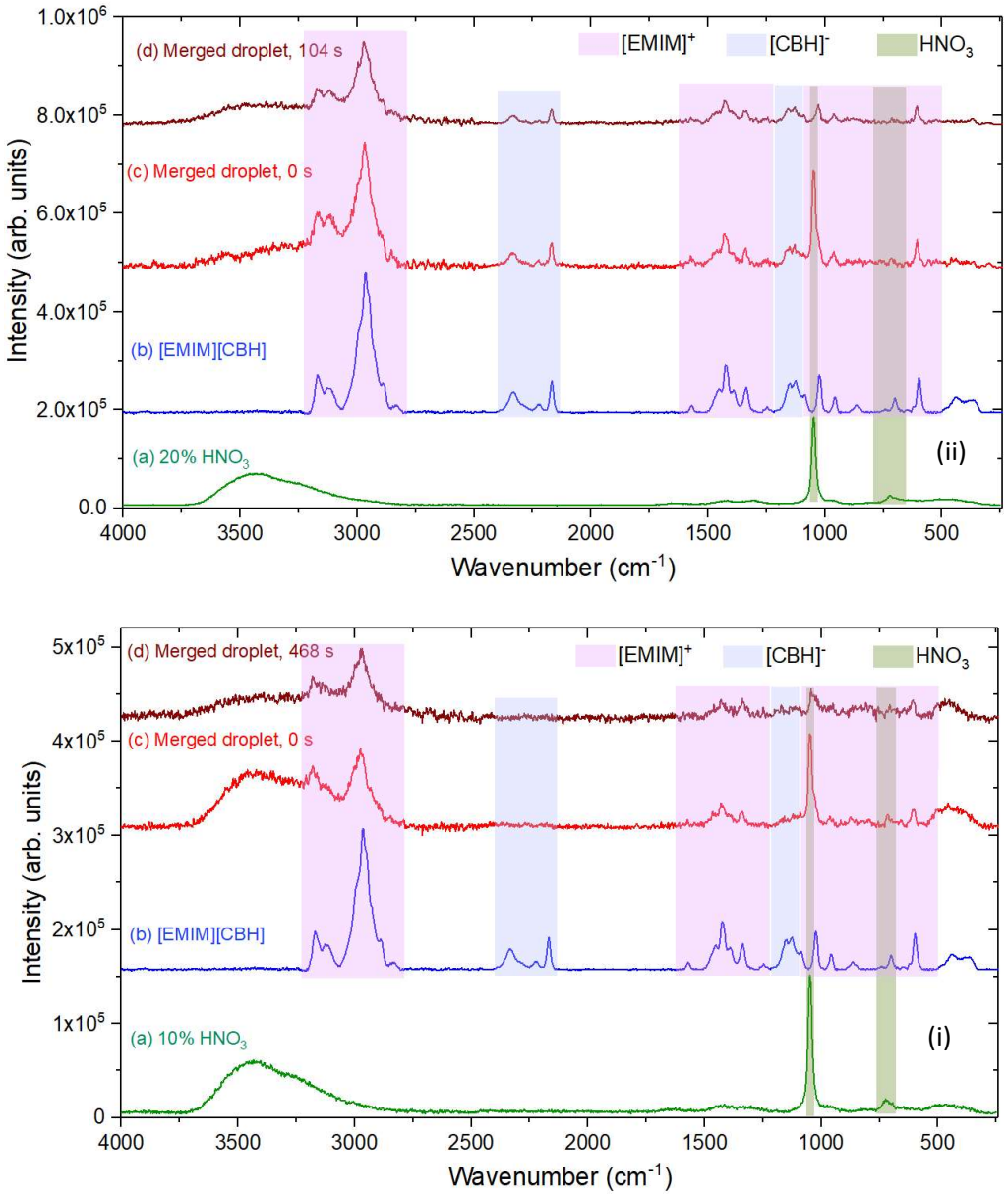

Figure S9. Raman spectra (c and d) of the merged droplet constituting the ionic liquid [EMIM][CBH] and aqueous solution of HNO_3 ((i) 10 % and (ii) 20 % undergoing chemical reaction, - (c) at merging and (d) after the reaction. In each of the plots, the Raman spectra for the reactants, (a) HNO_3 and (b) [EMIM][CBH] are also presented in the traces below. The characteristic regions of vibrational bands for the cationic ($EMIM^+$) and anionic (CBH^-) components of the ionic liquid, and the acid are highlighted using different color code.

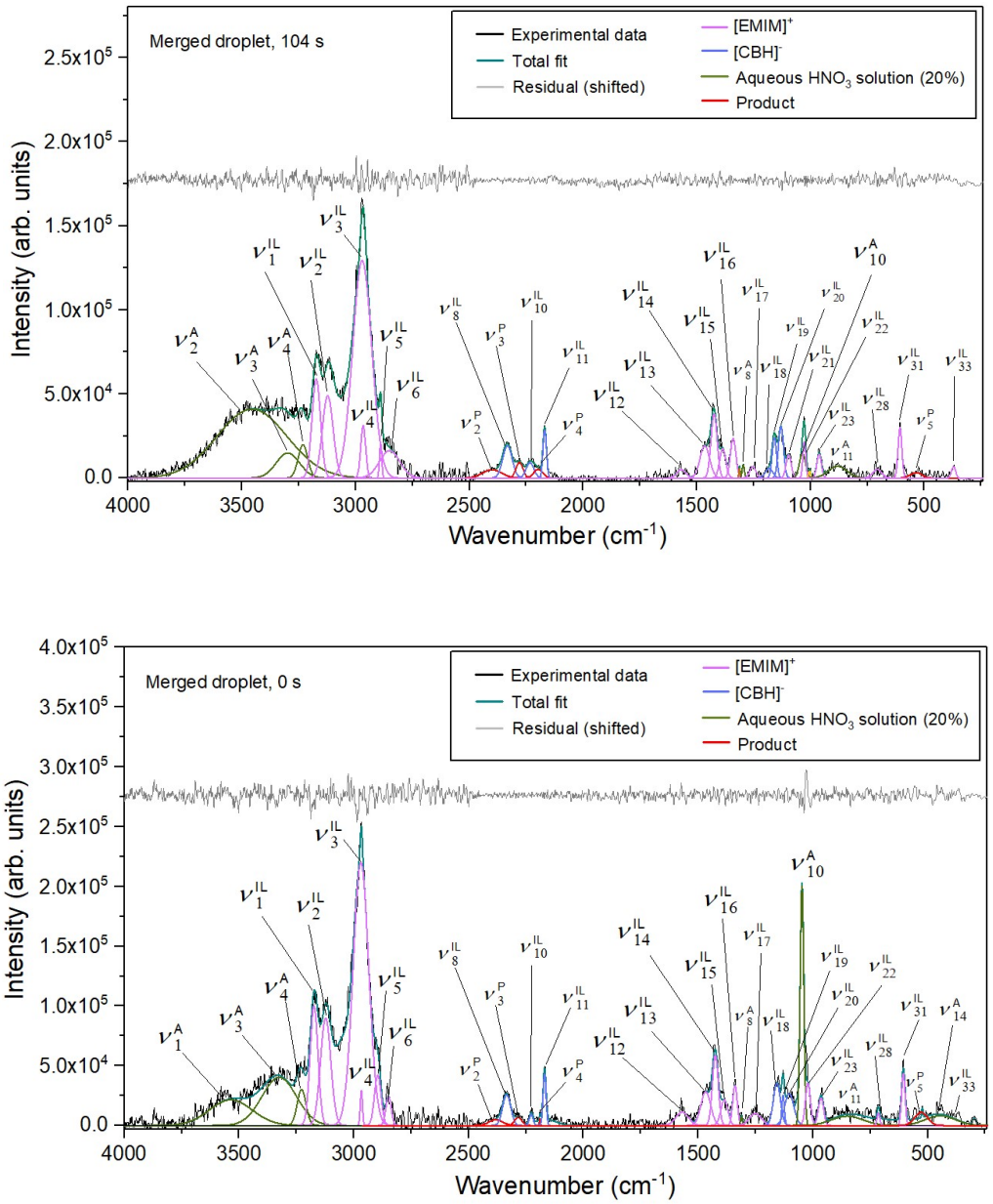

Figure S10. Deconvoluted spectra for the merged droplet constituting the ionic liquid [EMIM][CBH] and aqueous solution of 20 % HNO_3 undergoing chemical reaction, - at 0 s and 104 s from the merging. The features corresponding to the reactants and the newly formed products/intermediates are distinguished using different color codes and they are labelled with the superscripts, IL (ionic liquid), A (acid) and P (product) for each band (ν).

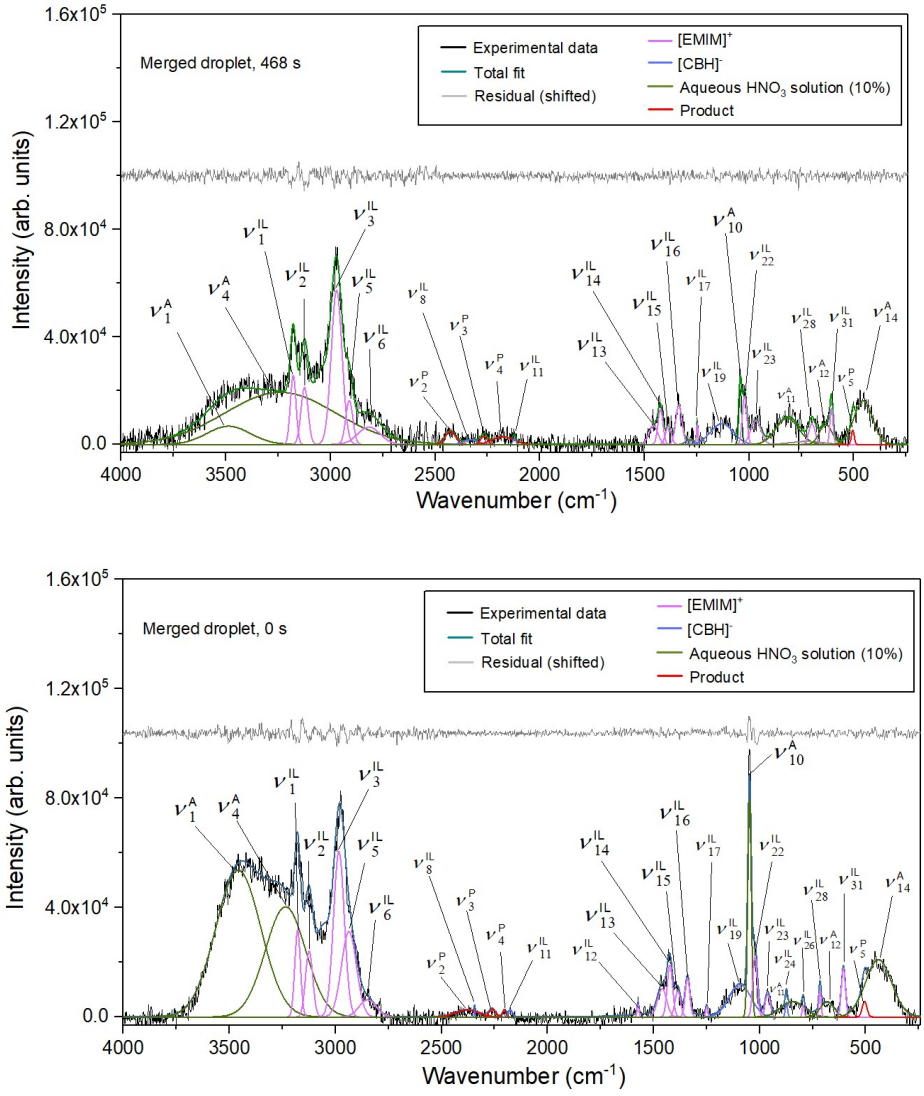

Figure S11. Deconvoluted spectra for the merged droplet constituting the ionic liquid [EMIM][CBH] and aqueous solution of 10 % HNO_3 undergoing chemical reaction, - at 0 s and 468 s from the merging. The features corresponding to the reactants and the newly formed products/intermediates are distinguished using different color codes and they are labelled with the superscripts, IL (ionic liquid), A (acid) and P (product) for each band (ν).

(i) Reactants

(A) 20% HNO_3 bands

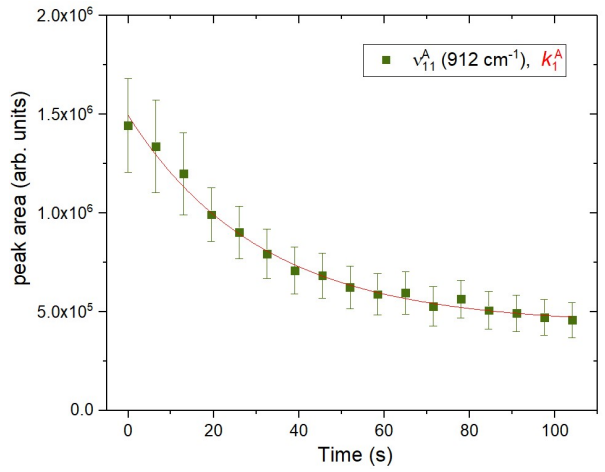

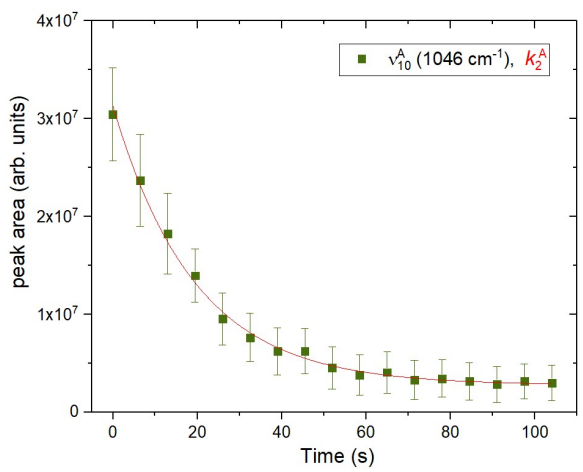

(B) Ionic liquid: anion bands

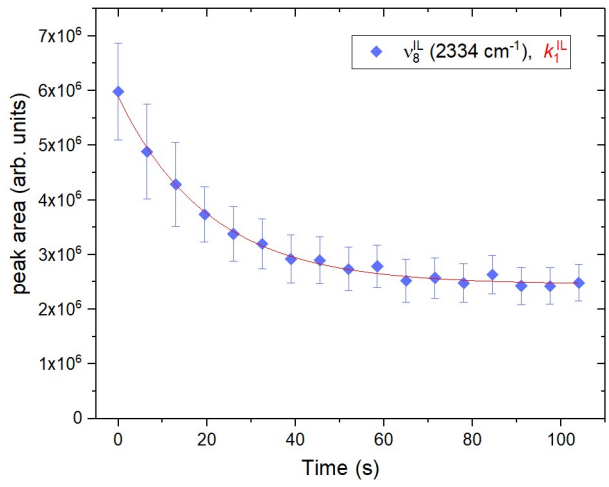

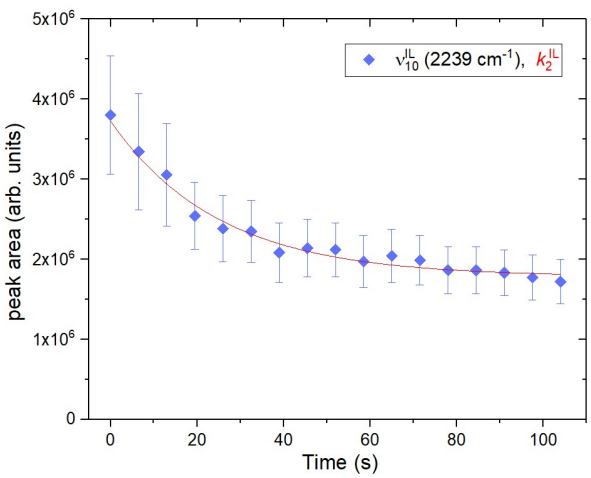

(C) Ionic liquid: cation bands

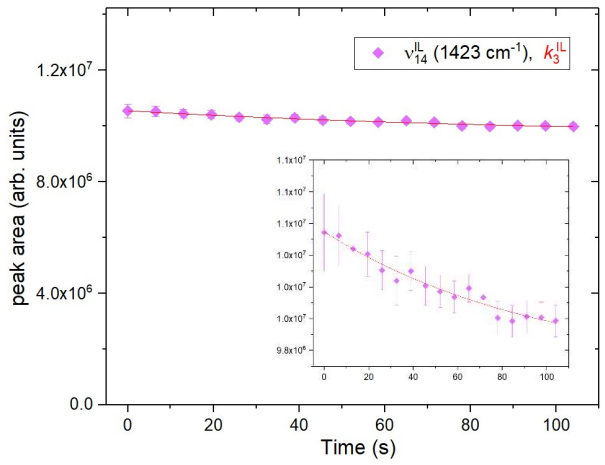

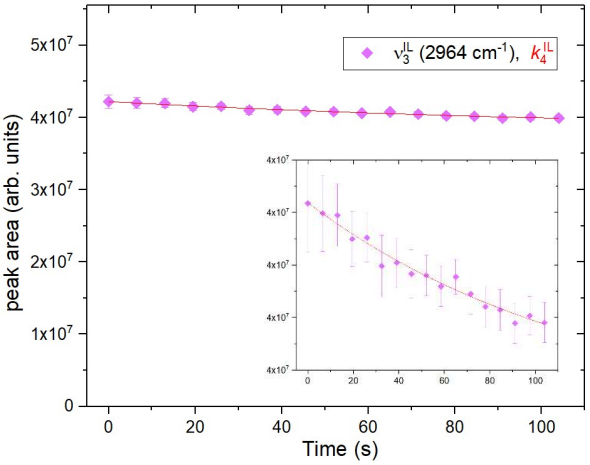

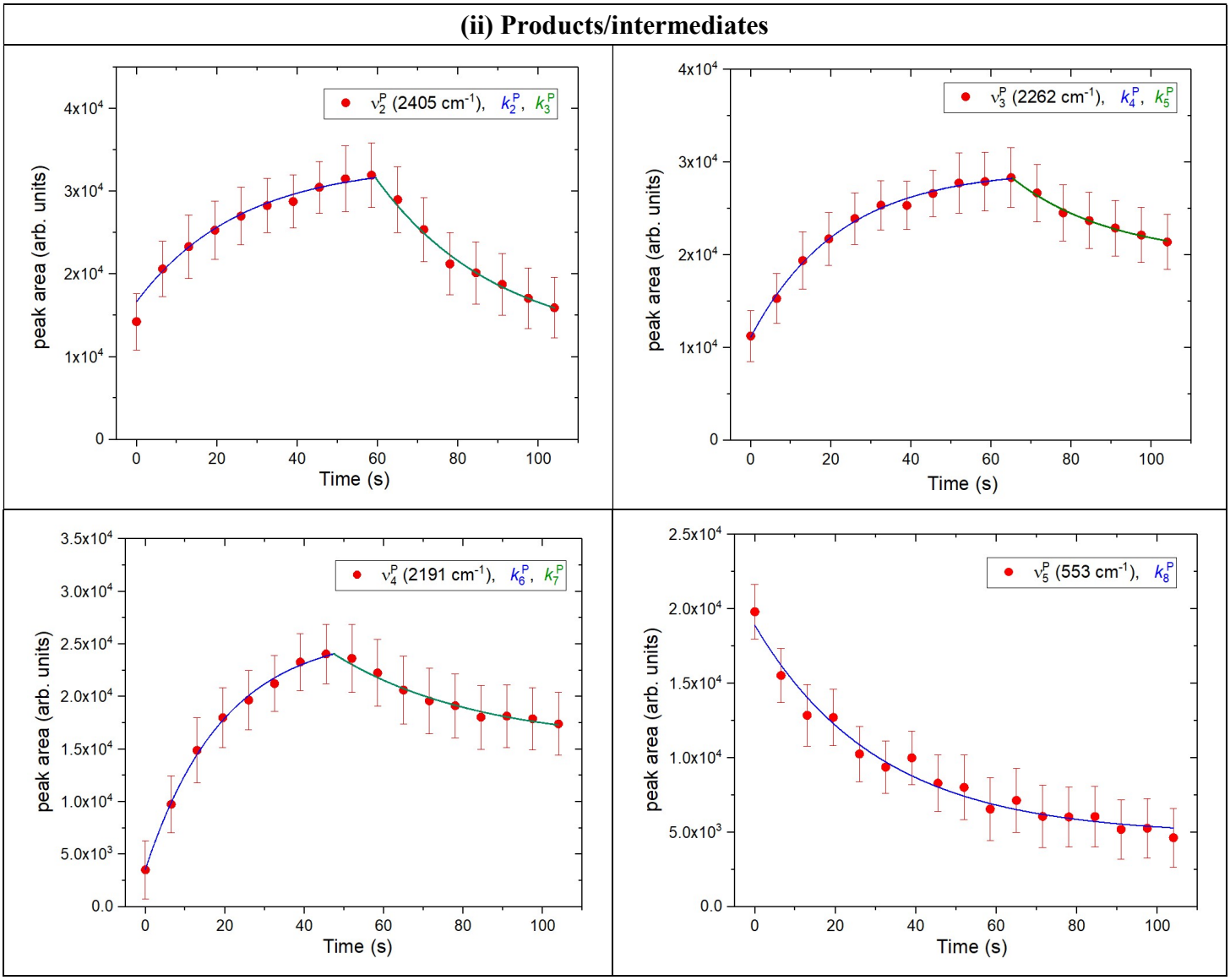

Figure S12. Temporal profiles for the select bands of the (i) reactants and (ii) products/intermediates in the Raman spectra which arise due to chemical reaction for the merged droplet constituting the ionic liquid [EMIM][CBH] and aqueous solution of 20 % HNO_3.

(i) Reactants

(A) 10% HNO_3 bands

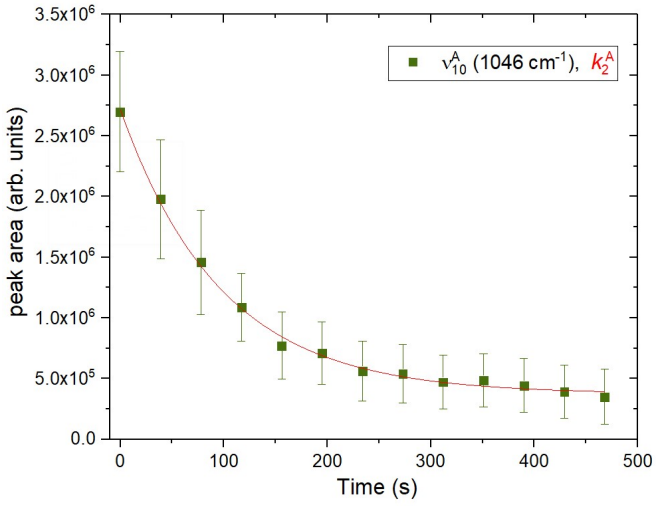

(B) Ionic liquid: anion bands

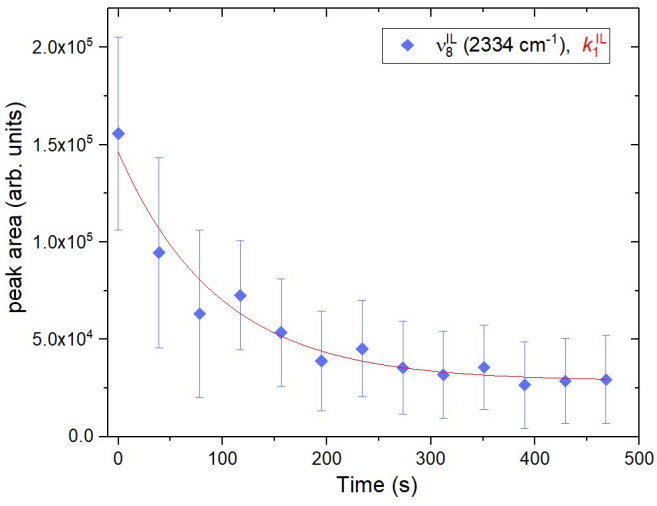

(C) Ionic liquid: cation bands

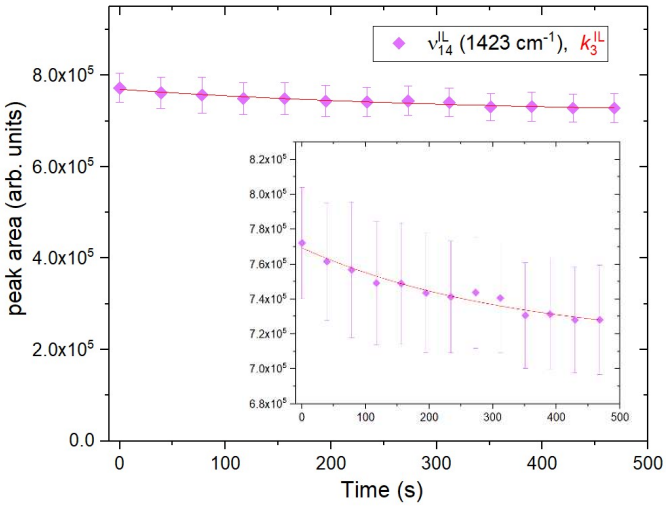

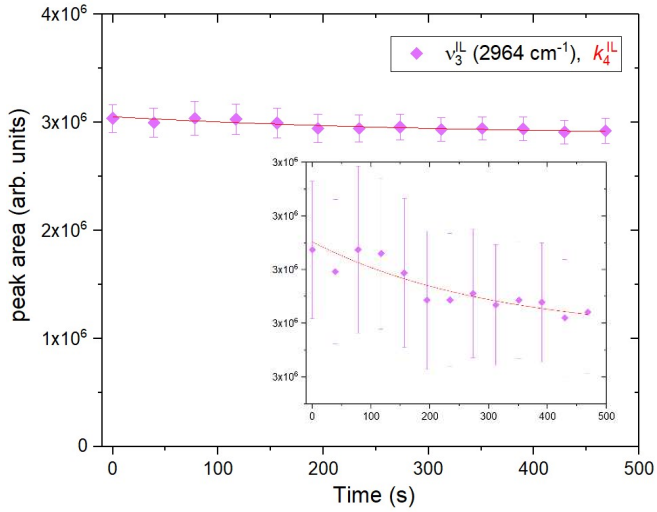

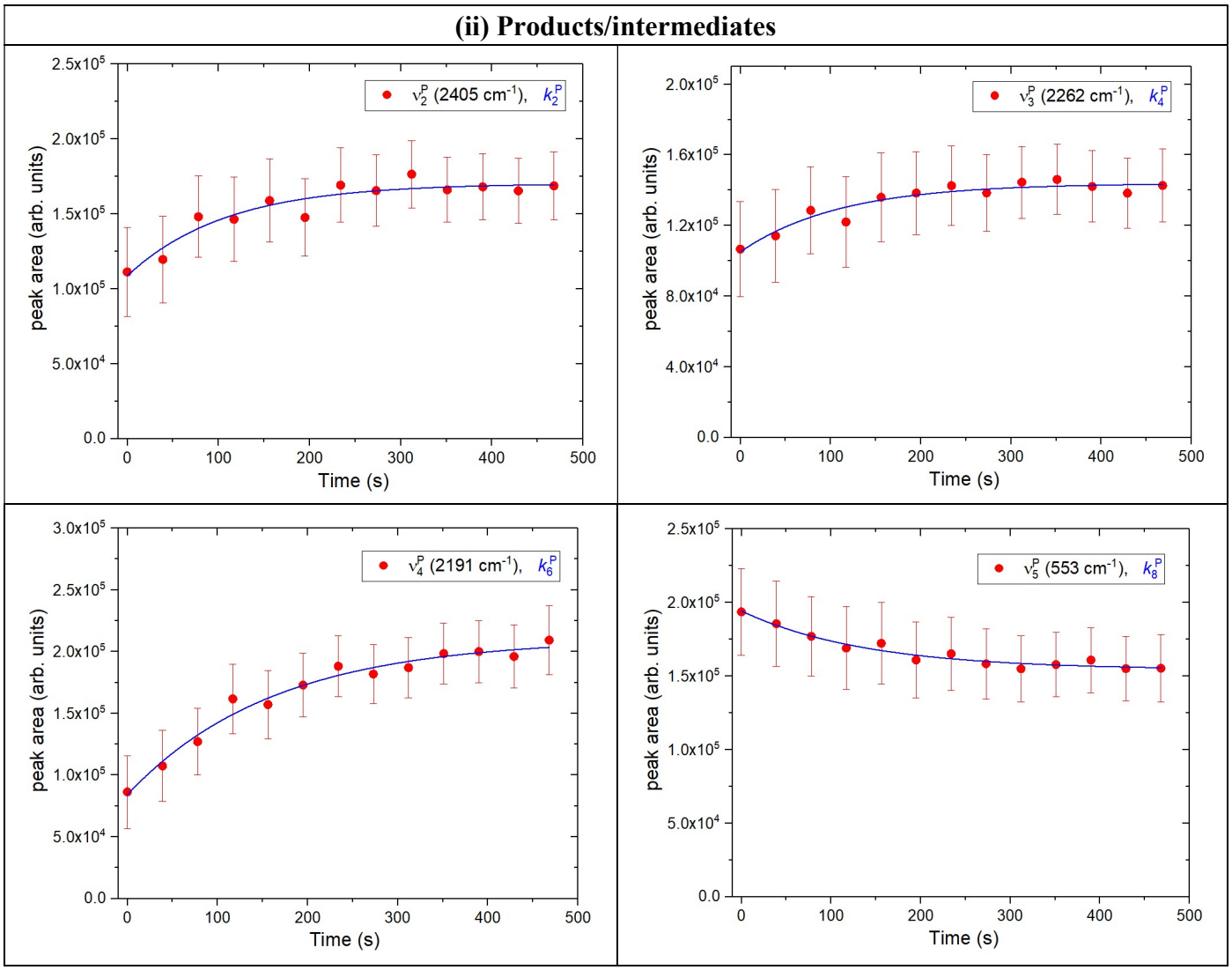

Figure S13. Temporal profiles for the select bands of the (i) reactants and (ii) products/intermediates in the Raman spectra which arise due to chemical reaction for the merged droplet constituting the ionic liquid [EMIM][CBH] and aqueous solution of 10 % HNO_3.

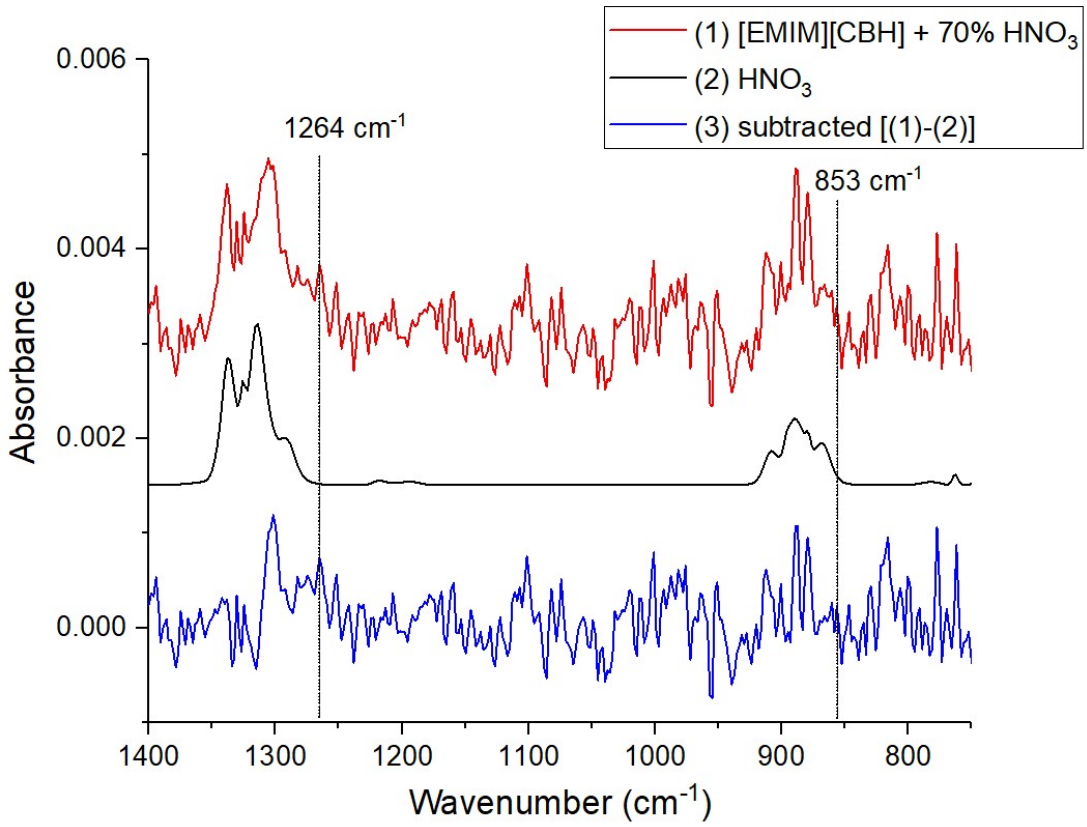

Figure S14. The reference spectrum for HNO_3 (trace 2) is subtracted from the FT-IR spectra of the gas-phase products formed in the reaction of the hypergolic ionic liquid [EMIM][CBH] and 70 % HNO_3 to locate the features of nitrous acid (HONO), which is computationally predicted to be one of the candidates to form. The characteristic wavenumbers (1264 and 853 cm^{-1}) of HONO are marked for convenience.[2] However, we could only tentatively show the appearance of the 1264 cm^{-1} band, the other band at 853 cm^{-1} could not be detected.

References:

1. Y. U. Paulechka, A. G. Kabo, A. V. Blokhin, G. J. Kabo and M. P. Shevelyova, *J. Chem. Eng. Data*, 2010, **55**, 2719-2724.
2. R. H. Kagann and A. G. Maki, *J. Quant. Spectrosc. Radiat. Transf.*, 1983, **30**, 37-44.